Terahertz quantum-cascade laser at λ≈100 μm using metal waveguide for mode confinement

Benjamin S. Williams, Sushil Kumar, Hans Callebaut, and Qing Hu[a)]
Department of Electrical Engineering and Computer Science and Research Laboratory of Electronics, Massachusetts Institute of Technology, Cambridge, Massachusetts 02139

John L. Reno
Sandia National Laboratories, Department 1123, MS 0601, Albuquerque, New Mexico 87185-0601

(Received 5 May 2003; accepted 30 July 2003)

We report lasing at ~3.0 THz (λ≈98–102 μm) in a quantum-cascade structure in which mode confinement is provided by a double-sided metal waveguide. The depopulation mechanism is based on resonant phonon scattering, as in our previous work. Lasing takes place in pulsed mode up to a heat-sink temperature of 77 K. The waveguide consists of metallic films placed above and below the 10-μm-thick multiple-quantum-well gain region, which gives low losses and a modal confinement factor of nearly unity. Fabrication takes place via low-temperature metallic wafer bonding and subsequent substrate removal using selective etching. This type of waveguide is expected to be increasingly advantageous at even longer wavelengths. © *2003 American Institute of Physics.* [DOI: 10.1063/1.1611642]

The development of the quantum-cascade laser (QCL)[1] has resulted in a class of semiconductor lasers in which the wavelength can be customized by engineering the multiple-quantum-well active region. These lasers have successfully spanned the mid-infrared frequency range, and recently far-infrared, or terahertz, QCLs have been demonstrated.[2–4] The underused terahertz frequency regime (1–10 THz, 30–300 μm) is the subject of increasing scientific and technological interest, and the development of compact coherent sources would be useful for applications such as spectroscopy and imaging.

Free carrier absorption grows increasingly strong at longer wavelengths, so that the development of a low-loss waveguide was critical for the realization of terahertz QCLs. An early design involved confinement between the upper metallic contact and a thick semiconductor layer heavily doped to act as a "metal" ($\Re\{\epsilon\}<0$).[5] However, even at the largest attainable doping level ($n\sim 5\times 10^{18}$ cm^{-3} in GaAs), the field penetrates significantly into the cladding, and hence free carrier losses are large.[6] Currently, all reported terahertz QCLs use a waveguide in which the mode is composed of surface plasmons bound to the upper metallic contact and a thin n^+ contact layer grown between the active region and the semi-insulating (SI) GaAs substrate.[2–4] Although the mode extends substantially into the substrate, the overlap with heavily doped regions is small, so that the free carrier loss is minimized. However, the mode confinement factor Γ is far below unity (Γ~0.2–0.5 for reported lasers). At longer wavelengths (λ>100 μm), Γ will become even smaller because of two factors. First, the geometric effect of a longer wavelength reduces the overlap. Second, the dielectric constant $\epsilon(\omega)$ in the lightly doped active region is reduced by a factor $1-\omega_p^2/\omega^2$ as the frequency ω approaches the plasma frequency $\omega_p=(ne^2/m^*\epsilon)^{1/2}$. The reduction of $\epsilon(\omega)$ in the active region compared to that of the SI substrate will further reduce the confinement factor.

In this letter, we report a terahertz QCL that uses a double-sided metal waveguide for mode confinement. This metal–semiconductor–metal structure is essentially the same as microstrip transmission lines that are widely used for waveguiding at microwave and millimeter-wave frequencies, and the geometry is compatible with the TM polarization of intersubband transitions. Due to the shallow skin depth in the metal, the waveguide can be made with very low losses and a confinement factor close to unity. Enhanced terahertz electroluminescence,[7] but not lasing, was observed in such a waveguide fabricated via Au-Au thermocompression bonding in Ref. 8. Mid-infrared QCLs have also been demonstrated using a metal waveguide fabricated via a solder-bonding method.[9]

The active region design is based around a vertical transition in which a combination of resonant tunneling and LO-phonon scattering is used to selectively depopulate the lower radiative state.[4] As shown in Fig. 1, the radiative transition takes place between levels $n=6$ and $n=5$ (highlighted with thicker lines), where the transition energy is calculated to be $E_{65}=11.4$ MeV. At the design bias (~61 meV/module), levels $n=5$ and $n=4$ are anticrossed ($E_{54}=5.2$ meV), and both levels are quickly depopulated through subpicosecond LO-phonon scattering ($\tau_5\approx\tau_4\approx 0.4$ ps) into the injector states ($n=3,2,1$). The small overlap between $n=6$ and the injector states limits the calculated parasitic scattering time to $\tau_{6\rightarrow(1,2,3)}\approx 6.0$ ps. The middle injector well is Si doped to provide a sheet electron density of 3.0×10^{10} cm^{-2}.

The cladding and contact layers were chosen so that the device could be processed using either a SI-surface-plasmon waveguide, or double-sided metal waveguide. The device wafer, FL152F, was grown using molecular beam epitaxy (MBE) on a SI GaAs substrate; first a 0.5-μm undoped $Al_{0.5}Ga_{0.5}As$ etch-stop layer was grown, then a 0.6-μm GaAs contact layer doped at $n=2\times 10^{18}$ cm^{-3}. Next, 152 cas-

a)Electronic mail: qhu@mit.edu

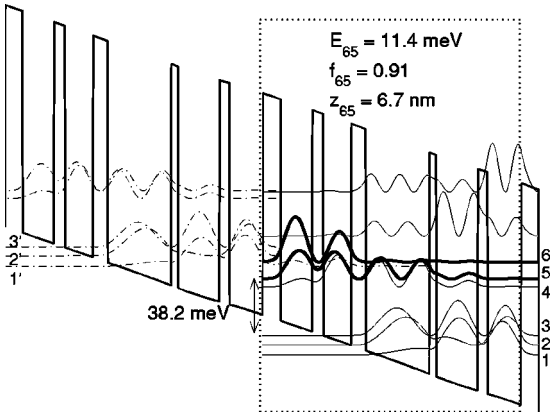

FIG. 1. Conduction band profile at a field of 9.5 kV/cm (60.5 mV/module) calculated using a self-consistent Schrödinger and Poisson solver. The device is grown in the $Al_{0.15}Ga_{0.85}As/GaAs$ material system and the five-well module is outlined by the dotted box. Beginning with the left injection barrier, the layer thicknesses in Å are 44/77/28/69/36/157/17/102/25/83. The 102-Å well is doped at $n=2.9\times10^{16}$ cm^{-3}, which yields a sheet density of $n=3.0\times10^{10}$ cm^{-2} per module.

caded modules were grown to form the 10-μm-thick active region. A 60-nm GaAs contact layer ($n=5\times10^{18}$ cm^{-3}) was grown above the active region, followed by a thin, low-temperature-grown GaAs cap layer to allow for the use of a nonalloyed ohmic contact. Fabrication of the SI-surface-plasmon waveguide structure took place via wet etching, as described in Ref. 4.

The double-sided metal waveguide was fabricated using low-temperature In-Au metallic wafer bonding followed by substrate removal. The schematic of the bonding process is shown in Fig. 2. Before bonding, the MBE-grown wafer was prepared by evaporating Ti/Au layers (20/1000 nm). An n^+ GaAs receptor substrate was coated with the metal sequence Pd/Ge/Pd/In/Au (25/10/25/1200/120 nm). The purpose of the Pd/Ge/Pd multilayer was to improve the electrical contact to the receptor substrate.[10] The topmost gold layer minimizes indium oxidation. Wafer pieces of about 1 cm^2 were cleaved, aligned, and bonded on a hot plate at 250 °C for 10 min while pressure was applied to the stack. Bonding takes place above the melting point of In (156.6 °C) as the indium wets the surface to fill in any crevices, and then diffuses into the gold layer to reactively form a variety of In-Au alloys.[11,12]

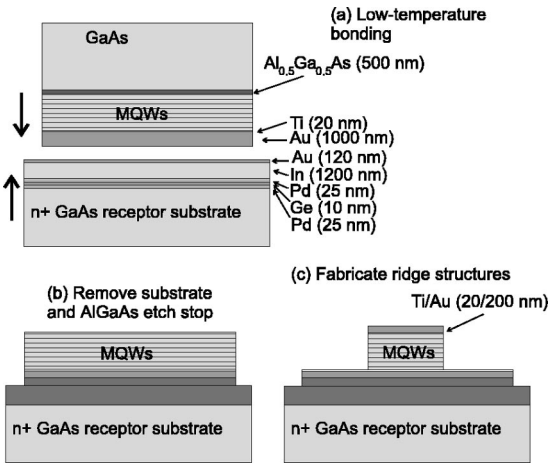

FIG. 2. Schematic for the wafer bonding processing for double-sided metal waveguide.

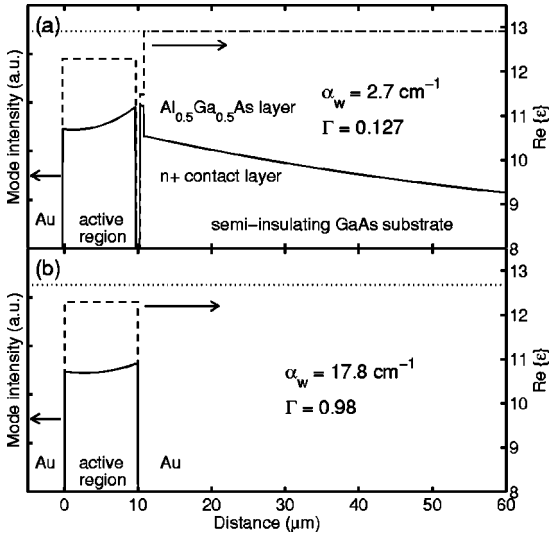

FIG. 3. Mode intensities (solid lines) and the real part of the dielectric constant $\epsilon(\omega)$ (dashed lines) for the (a) SI-surface-plasmon waveguide and (b) double-sided metal waveguide. The dotted line represents the square of the modal effective index.

By careful choice of layer thicknesses, all the indium is consumed, and the bonding layer remains robust up to the melting points of the In-Au alloys ($\sim$450 °C).

The SI GaAs substrate was first lapped and then chemically removed in $NH_4OH:H_2O_2$ (1:19). This selective etch stopped at the $Al_{0.5}Ga_{0.5}As$ layer, which was subsequently removed in HF acid. To reduce free carrier absorption, the 0.6-μm n^+ contact layer was etched to a thickness of approximately 0.2 μm. Ti/Au (20/400 nm) contacts were evaporated using a lift-off process and then used as self-aligned etch masks to define ridge structures of various widths. Electron cyclotron resonance reactive ion etching in a $BCl_3:N_2$ gas mixture was used to etch down to the underlying metal. Finally, Ti/Au was deposited on the wafer backside, the devices were cleaved, and Al_2O_3/Ti/Au layers (approximately 300/15/150 nm) were evaporated on the back facets to form a high reflectivity (HR) coating. The resulting metal waveguide structure was sufficiently mechanically strong to allow multiple wire bonds to be made directly to the top of the ridge.

The one-dimensional mode patterns for the two waveguides were calculated using a Drude model solver and are shown in Fig. 3. Drude scattering times of $\tau=0.1$ ps and 0.5 ps were used for the heavily doped and lightly doped semiconductor regions, respectively, and $\tau=0.05$ ps was used for gold.[13] The SI-surface-plasmon waveguide was calculated to have a waveguide loss of $\alpha_w=2.7$ cm^{-1} and a confinement factor of $\Gamma=0.127$. The $Al_{0.5}Ga_{0.5}As$ layer, which is not normally present in SI-surface-plasmon waveguides, causes a slight reduction in confinement and loss. The metal waveguide was calculated to have $\alpha_w=17.8$ cm^{-1} and $\Gamma=0.98$. Only about 6 cm^{-1} of that loss is due to the metal and contact layers, and the remainder is due to free carrier absorption in the active region. The expression for the threshold material gain g is given by

$$g=\alpha_w/\Gamma+\alpha_m/\Gamma, \tag{1}$$

where α_m is the mirror loss. Since α_m ranges from roughly

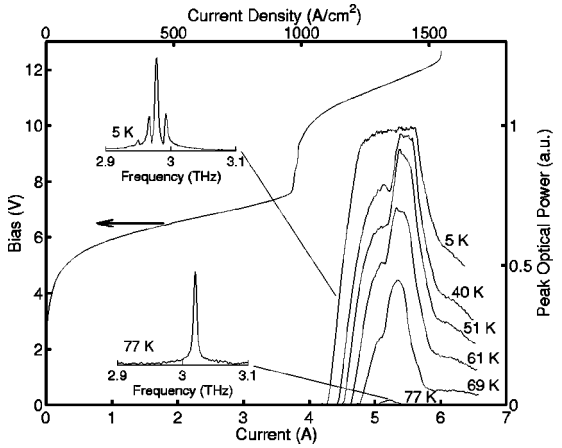

FIG. 4. Applied bias versus current at 5 K and emitted light versus current at various temperatures, measured using 100-ns pulses repeated at 1 kHz. Note that the $I-V$ characteristic was measured using a similar, but smaller device, so only the current density scale is applicable. Spectra taken at 5 and 77 K (with liquid nitrogen cooling) using 100-ns pulses repeated at 10 kHz are also shown. Emitted light was measured using a Ge:Ga photodetector, and the spectra were collected using a Nicolet 850 Fourier transform infrared spectrometer operated in linear-scan mode with a resolution of $0.125\ \mathrm{cm}^{-1}$.

$2-10\ \mathrm{cm}^{-1}$ for typical cavity lengths, it is clear that the large confinement factor is a major advantage, because while the term α_w/Γ is of similar magnitude for both waveguides, the term α_m/Γ can become quite large for the SI-surface-plasmon waveguide.

Devices were indium soldered ridge side up on a copper mount on a cold finger in a vacuum cryostat. Lasing was observed in a 150-μm-wide, 2.59-mm-long metal waveguide device in pulsed mode up to a heat sink temperature of 77 K. Light versus current relations and spectra for this device are shown in Fig. 4. At 5 K, emission takes place from 2.94 THz ($\lambda=102\ \mu$m) to 3.06 THz ($\lambda=98\ \mu$m) as the bias is increased. At 77 K emission is single mode at 3.02 THz, and the spectrum was taken with the laser cooled by liquid nitrogen. The emission corresponds to a transition energy of 12.4 meV, slightly larger than the calculated value of 11.4 meV. The threshold current density at 5 K is $J_{\mathrm{th}}=1100\ \mathrm{A\,cm}^{-2}$, and the peak power is estimated to be roughly 100 μW. The high value of J_{th} is a result of a parasitic current channel from $n=1',2'$ into $n=4$ that dominates transport for $J\leqslant 1000\ \mathrm{A\,cm}^{-2}$, which gives rise to the shoulder-like feature in the $V-I$ at a bias of ~ 7 V (see Ref. 14). Not until beyond this bias point does the injector line up with the upper radiative state $n=6$ to give gain. The maximum duty cycle is limited, as lasing occurs only over the first 2 μs of an applied pulse. This effect is likely related to device heating during operation, due to the relatively high threshold current density. Using thicker barriers in the injector region should reduce the parasitic channel and thus the threshold current density. Such an improvement should yield a more robust laser performance at high duty cycles.

Nonetheless, the observation of terahertz lasing using a metal waveguide confirms its effectiveness for long wavelength operation. Devices of similar dimensions (150-μm wide and 2.7-mm long, HR coated) that were fabricated using the SI-surface-plasmon waveguide failed to lase. Metal waveguides become increasingly advantageous for longer wavelengths, whereas the confinement factor Γ for the SI-surface-plasmon waveguide decreases even further. The reduction in Γ is due both to a geometric effect as the wavelength grows relative to the active region thickness, and to the $1-\omega_p^2/\omega^2$ reduction of the dielectric constant in the active region. As a result of this reduction in $\Re\{\epsilon(\omega)\}$ by the free carriers, the mode extends further into the substrate where the dielectric constant is higher [Fig. 3(a)], or even becomes unbound below some cutoff frequency (2.8 THz at our doping level in the active region). It should be pointed out that this calculated reduction of $\epsilon(\omega)$ may even be an underestimate. The intersubband transitions in the injector region shift the oscillator strength to higher frequencies than predicted by the Drude model, potentially yielding an greater reduction in $\epsilon(\omega)$.[15] The reduction in Γ may be mitigated by increasing the thickness of the n^+ contact layer, or by decreasing the active region doping, but this comes at the cost of increased loss or reduced design flexibility. On the other hand, Γ for the double-sided metal waveguide is always close to unity regardless of the doping concentration in the active region. This important advantage will be valuable or even crucial in the effort to extend quantum-cascade laser operation to even longer wavelengths.

This work is supported by AFOSR, NASA, and NSF. Sandia is a multiprogram laboratory operated by Sandia Corporation, a Lockheed Martin Company, for the United States Department of Energy under Contract DE-AC04-94AL85000.

[1] J. Faist, F. Capasso, D. L. Sivco, C. Sirtori, A. L. Hutchinson, and A. Y. Cho, Science **264**, 553 (1994).
[2] R. Köhler, A. Tredicucci, F. Beltram, H. E. Beere, E. H. Linfield, A. G. Davies, D. A. Ritchie, R. C. Iotti, and F. Rossi, Nature (London) **417**, 156 (2002).
[3] M. Rochat, L. Ajili, H. Willenberg, J. Faist, H. Beere, G. Davies, E. Linfield, and D. Ritchie, Appl. Phys. Lett. **81**, 1381 (2002).
[4] B. S. Williams, H. Callebaut, S. Kumar, Q. Hu, and J. L. Reno, Appl. Phys. Lett. **82**, 1015 (2003).
[5] Q. Hu and S. Feng, Appl. Phys. Lett. **59**, 2923 (1991).
[6] M. Rochat, M. Beck, J. Faist, and E. Oesterle, Appl. Phys. Lett. **78**, 1967 (2001).
[7] B. S. Williams, Ph.D. thesis, Massachusetts Institute of Technology (2003).
[8] B. Xu, Ph.D. thesis, Massachusetts Institute of Technology, 1998.
[9] K. Unterrainer, R. Colombelli, C. Gmachl, F. Capasso, H. Y. Hwang, A. M. Sergent, D. L. Sivco, and A. Y. Cho, Appl. Phys. Lett. **80**, 3060 (2002).
[10] L. C. Wang, X. Z. Wang, S. S. Lau, T. Sands, W. K. Chen, and T. F. Kuech, Appl. Phys. Lett. **56**, 2129 (1990).
[11] C. C. Lee, C. Y. Wang, and G. Matijasevic, IEEE Trans. Compon., Hybrids, Manuf. Technol. **16**, 311 (1993).
[12] T. B. Wang, Z. Z. Shen, R. Q. Ye, X. M. Xie, F. Stubhan, and J. Freytag, J. Electron. Mater. **29**, 443 (2000).
[13] Landolt-Börnstein, *Numerical Date and Functional Relationships in Science and Technology*, edited by K.-H. Hellwege and O. Madelung (Springer, Berlin, 1985), Vol. III/15b, Chap. 4, pp. 210–222.
[14] H. Callebaut, S. Kumar, B. S. Williams, Q. Hu, and J. L. Reno, Appl. Phys. Lett. **83**, 207 (2003).
[15] T. Ando, A. B. Fowler, and F. Stern, Rev. Mod. Phys. **54**, 437 (1982).